Comparison of EKF and UKF for spacecraft localization via angle measurements

Antonio Giannitrapani *Member, IEEE*, Nicola Ceccarelli,

Fabrizio Scortecci, Andrea Garulli *Senior Member, IEEE*

Abstract

In this paper, the performance of two nonlinear estimators is compared for the localization of a spacecraft. It is assumed that range measurements are not available (like in deep space missions) and the localization problem is tackled on the basis of angles-only measurements. A dynamic model of the spacecraft accounting for several perturbing effects, such as Earth and Moon gravitational field asymmetry and errors associated with the Moon ephemerides, is employed. The measurement process is based on elevation and azimuth of Moon and Earth with respect to the spacecraft reference system. Position and velocity of the spacecraft are estimated by using both the Extended Kalman Filter (EKF) and the Unscented Kalman Filter (UKF). The behavior of the filters is compared on two sample missions: Earth-to-Moon transfer and geostationary orbit raising.

Index Terms

Spacecraft localization, Nonlinear estimation, Extended Kalman Filter, Unscented Kalman Filter.

I. Introduction

Nonlinear estimation techniques play a crucial role in any autonomous navigation system (e.g., see [1], [2], [3]). It is a fact that many of the problems to be faced in order to achieve full autonomy can be

Antonio Giannitrapani and Andrea Garulli are with the Dipartimento di Ingegneria dell'Informazione, Università di Siena, Siena, Italy. Email: {giannitrapani,garulli}@dii.unisi.it.

Nicola Ceccarelli, formerly with the Dipartimento di Ingegneria dell'Informazione, Università di Siena, is now with GE Oil & Gas, Firenze, Italy. Email: nicola.ceccarelli@gmail.com.

Fabrizio Scortecci is with AEROSPAZIO Tecnologie s.r.l., Rapolano Terme, Siena, Italy. Email: fscortecci@aerospazio.com.

cast as estimation problems. Among others, the ability of estimating the position of a spacecraft from the information provided by its onboard sensors (localization problem) is of paramount importance for the success of any mission.

This is especially true when dealing with spacecraft propelled by electric propulsion systems (EPS). Small and cheap electrically propelled spacecraft have recently gained a growing interest for lunar and outer planetary explorations, after the the successful SMART-1 mission of the European Space Agency [4], [5]. The use of EPS for the final stint of satellite launching (so called Chemical-Electric missions for Orbit Raising, C-EOR) is more and more adopted by companies, thanks to their good trade-off between on-orbit delivery time and propellant required [6]. However, the low thrust produced by a EPS leads to a continuous thrusting strategy which, in turn, requires an accurate knowledge of the spacecraft position and attitude during the transfer orbit. Therefore, accurate localization capabilities become a fundamental requirement for this type of missions.

Localization of spacecraft is usually very accurate when GPS range measurements are available [2]. The problem becomes more challenging when GPS signals are not available, like in high-Earth orbits or in long range missions, such as Earth-to-Moon transfers. In these cases, spacecraft navigation is often handled by ground-based tracking stations, thus making it unfeasible for low-cost spacecraft missions. In order to make spacecraft fully autonomous, it is necessary to devise self-localization and navigation algorithms relying only on measurements provided by onboard sensors [3], [7].

In this paper, the problem of spacecraft self-localization is addressed using angular measurements. First, a dynamic model of the spacecraft is formulated, which takes into account several perturbing effects such as Earth and Moon gravitational field asymmetry and errors associated with the Moon ephemerides (see e.g. [8], [9]). It is assumed that the navigation system is able to estimate the spacecraft attitude (by using a star tracker sensor [10]), and the spacecraft is equipped with line of sight sensors providing measurements of elevation and azimuth of Moon and Earth with respect to the spacecraft reference system (see e.g. [11], [12]). Range measurements, which are often difficult to obtain or not sufficiently reliable, are not required. Then, position and velocity of the spacecraft are estimated by employing both the classical Extended Kalman Filter (EKF) [13] and the recently developed Unscented Kalman Filter (UKF) [14]. Comparisons between EKF and UKF have been proposed in several contexts, ranging from target tracking [15], [16], to positioning systems [17], [18] , virtual reality [19]. The filters have been tested on simulated data concerning two different missions (Earth-to-Moon transfer and GEO orbit raising). The resulting localization errors, and the associated confidence intervals, show that the proposed algorithms provide reliable estimates, whose accuracy is sufficient for autonomous navigation in the considered class of missions. Preliminary results have been presented in [20].

The paper is organized as follows. In Section II the spacecraft dynamic model and the measurement process are introduced. The localization problem is formulated in Section III, and the adopted nonlinear estimators are briefly recalled. Section IV reports results from numerical simulations of a Earth-to-Moon transfer and a geostationary orbit raising. Finally, some conclusions are drawn in Section V.

II. Spacecraft model

The following dynamic model for the spacecraft is considered

$$\ddot{\mathbf{r}} = -\frac{\mu}{\rho^3}\mathbf{r} + \mu_m\left(\frac{\mathbf{r}_{sm}}{\rho_{sm}^3} - \frac{\mathbf{r}_m}{\rho_m^3}\right) + \frac{\mathbf{T}}{m} \quad (1)$$

$$\dot{m} = -\frac{||\mathbf{T}||}{I_{sp}\ g}, \quad (2)$$

where $\mathbf{r} = [x,\ y,\ z]'$, $\mathbf{r}_m = [x_m,\ y_m,\ z_m]'$ are the spacecraft and Moon positions in the Earth Centered Inertial reference system (ECI [21]), see Figure 1. In equations (1)-(2), $\mu = 398600.4415\ km^3/s^2$ and $\mu_m = 4902.801\ km^3/s^2$ are the gravitational parameters; $\rho = \|\mathbf{r}\|$, $\rho_m = \|\mathbf{r}_m\|$ are the distances of the spacecraft and the Moon from the earth, respectively; $\mathbf{r}_{sm} = \mathbf{r}_m - \mathbf{r}$ is the moon position with respect to the spacecraft, and $\rho_{sm} = \|\mathbf{r}_{sm}\|$. The vector $\mathbf{T}$ denotes the thrust provided by the propulsion system, m is the spacecraft mass, and I_{sp} is the specific impulse [21].

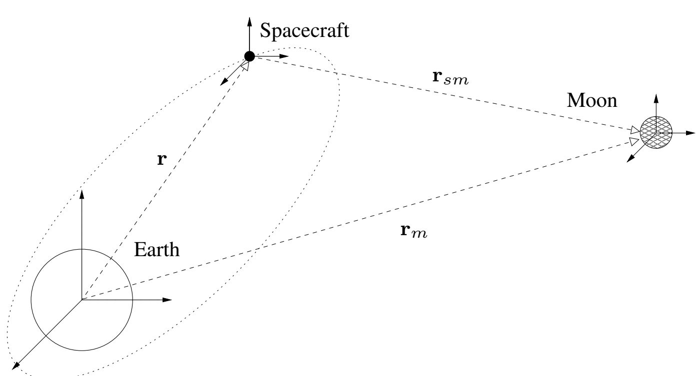

Fig. 1. The ECI reference system

If we define the state vector

$$\mathbf{X} = [x,\ y,\ z,\ \dot{x},\ \dot{y},\ \dot{z},\ m]' \tag{3}$$

containing the spacecraft position and velocity, as well as its mass, model (1)-(2) can be rewritten in vector form as

$$\dot{\mathbf{X}} = f(\mathbf{X}, \mathbf{u}_1, \mathbf{u}_2), \tag{4}$$

where the inputs are the motor thrust and the Moon position,

$$\mathbf{u}_1 = \mathbf{T},$$

$$\mathbf{u}_2 = \mathbf{r}_m.$$

In order to make a fair and easy-to-implement comparison between EKF and UKF, equation (4) is discretized with sampling time Δ_T (UKF is typically applied to discrete-time systems and its extension to continuous-time systems is the subject of ongoing research, see [22] for a recent contribution). The Euler forward discretization of the continuous-time dynamics (4) is given by

$$\mathbf{X}_{(k+1)\Delta_T} = \mathbf{X}_{k\Delta_T} + \Delta_T f(\mathbf{X}_{k\Delta_T}, \mathbf{u}_{1,k\Delta_T}, \mathbf{u}_{2,k\Delta_T}). \tag{5}$$

In the following, for ease of notation, we will get rid of the dependence on the sampling time Δ_T, and will denote by $\mathbf{q}_k$ the value of the quantity $\mathbf{q}$ at time $k\Delta_T$.

In a real-world scenario, there exist several sources of uncertainty affecting the deterministic model (5). First, at time $k\Delta_T$ inputs are not exactly known. Specifically, it is assumed that the propulsion system generates a perturbed thrust

$$\mathbf{u}_{1,k} = (1 + \omega_{u,k})\bar{\mathbf{T}}_k, \tag{6}$$

where $\bar{\mathbf{T}}$ denotes the nominal thrust and $\omega_{u,k}$ is a discrete-time white stochastic process. Notice that the thrust perturbation affects also the fuel mass evolution. Moreover, since also the location of the Moon is not exactly known, the Moon ephemerides algorithm [8] is used to estimate it. Hence, the knowledge of the Moon position is affected by the error $\mathbf{e}_{m,k} = [\epsilon_{m_x,k},\ \epsilon_{m_y,k},\ \epsilon_{m_z,k}]'$, where each component is a discrete-time white stochastic process. Therefore, if $\bar{\mathbf{r}}_m$ is the Moon position provided by the ephemerides, the actual second input becomes

$$\mathbf{u}_{2,k} = \bar{\mathbf{r}}_{m,k} + \mathbf{e}_{m,k}. \tag{7}$$

A second source of uncertainty is due to perturbing effects neglected in the nominal model, such as Earth and Moon gravitational field asymmetry, air drag and sun attraction [23]. According to Cowell's formulation, these contributions can be modeled by an additive process disturbance in the right hand side of (1) (see Sec. 8.4 in [8]). By including the perturbing effects and the input perturbations (6)-(7) into the nominal model (5), one obtains the perturbed discrete-time dynamic model

$$\mathbf{X}_{k+1} = \mathbf{X}_k + \Delta_T(f(\mathbf{X}_k, (1+\omega_{u,k})\bar{\mathbf{T}}_k, \bar{\mathbf{r}}_{m,k} + \mathbf{e}_{m,k}) + \mathbf{c}_k). \tag{8}$$

where

$$\mathbf{c}_k = [0,\ 0,\ 0,\ \bar{\mathbf{w}}_k',\ 0]', \tag{9}$$

and $\bar{\mathbf{w}}_k \in \mathbb{R}^3$. If we stack all the uncertainty sources of the dynamic model in a discrete-time disturbance vector

$$\mathbf{w}_k = [\bar{\mathbf{w}}_k',\ \omega_{u,k},\ \mathbf{e}_{m,k}']', \tag{10}$$

then the time evolution of the spacecraft dynamics can be written as

$$\mathbf{X}_{k+1} = f_d(\mathbf{X}_k, \bar{\mathbf{T}}_k, \bar{\mathbf{r}}_{m,k}, \mathbf{w}_k), \tag{11}$$

where $\bar{\mathbf{T}}_k$ and $\bar{\mathbf{r}}_{m,k}$ are known inputs, and the definition of $f_d(\cdot,\cdot,\cdot)$ follows from equations (1)-(4),(8)-(10).

The spacecraft is equipped with sensors that provide angular measurements of azimuth and elevation of Moon and Earth, with respect to a local reference system centered at the spacecraft and aligned to ECI, see Figure 2 (recall that it is assumed that the attitude of the spacecraft is known). Noise-free measurements at sampling instant k are related to the spacecraft and Moon position by the following equations

$$\theta_{e,k} = \text{atan}_2\left(-y_k, -x_k\right), \tag{12}$$

$$\phi_{e,k} = \text{atan}\left(\frac{-z_k}{\sqrt{x_k^2 + y_k^2}}\right), \tag{13}$$

$$\theta_{m,k} = \text{atan}_2\left(y_{m,k} - y_k, x_{m,k} - x_k\right), \tag{14}$$

$$\phi_{m,k} = \text{atan}\left(\frac{z_{m,k} - z_k}{\sqrt{(x_{m,k} - x_k)^2 + (y_{m,k} - y_k)^2}}\right), \tag{15}$$

where $\text{atan}_2(y, x) \in (-\pi,\ \pi]$ is the four-quadrant inverse tangent. Recalling that the Moon position $\mathbf{r}_{m,k}$ corresponds to the input $\mathbf{u}_{2,k}$, the equations above can be summarized as

$$\bar{\mathbf{Y}}_k = \bar{h}(\mathbf{X}_k, \mathbf{u}_{2,k}), \tag{16}$$

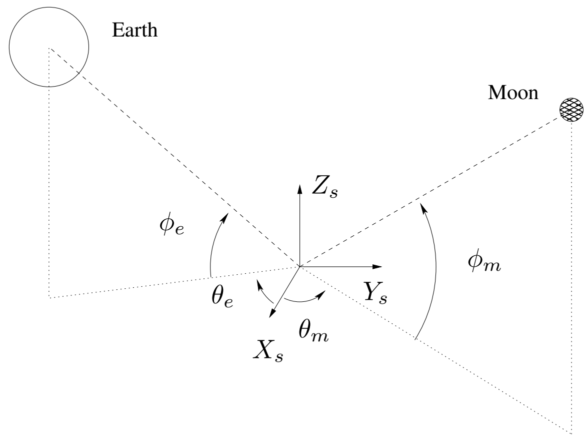

Fig. 2. Angle measurements in the spacecraft reference system

where $\bar{\mathbf{Y}} = [\theta_e \ \phi_e \ \theta_m \ \phi_m]'$ and $\bar{h}(\cdot,\cdot)$ is defined according to equations (12)-(15) and the definitions of $\mathbf{X}$ in (3). Now, by plugging equation (7) into (16), and taking into account the noise $\mathbf{n}_k$ affecting nominal measurements $\bar{\mathbf{Y}}_k$, the actual measurement equations become

$$\mathbf{Y}_k = \bar{h}(\mathbf{X}_k, \bar{\mathbf{r}}_{m,k} + \mathbf{e}_{m,k}) + \mathbf{n}_k, \tag{17}$$

where

$$\mathbf{n}_k = [v_{\theta_e,k}, \ v_{\phi_e,k}, \ v_{\theta_m,k}, \ v_{\phi_m,k}]' \tag{18}$$

is a discrete-time white noise modeling measurement errors. If we group all the error source entering in equation (17) in the noise vector

$$\mathbf{v}_k = [\mathbf{n}_k', \ \mathbf{e}_{m,k}']', \tag{19}$$

the measurement equation can be rewritten as

$$\mathbf{Y}_k = h(\mathbf{X}_k, \bar{\mathbf{r}}_{m,k}, \mathbf{v}_k), \tag{20}$$

where $\bar{\mathbf{r}}_{m,k}$ is a known signal (the Moon ephemerides), and the definition of $h(\cdot,\cdot,\cdot)$ follows from equations (12)-(19). Notice that the error on the Moon position estimates, coming from the ephemerides algorithm, enters both the discrete-time process disturbance $\mathbf{w}_k$ and the discrete-time measurement noise $\mathbf{v}_k$, see equations (10) and (19).

III. State estimation

The estimation of the spacecraft position and velocity boils down to the state estimation problem for system (11), based on the observations (20). In this section, we will briefly recall the equations of the estimators that will be adopted in this work. To this purpose, we will refer to the discrete-time model

$$\begin{aligned} \mathbf{X}_{k+1} &= f_d(\mathbf{X}_k, \bar{\mathbf{T}}_k, \bar{\mathbf{r}}_{m,k}, \mathbf{w}_k), \\ \mathbf{Y}_k &= h(\mathbf{X}_k, \bar{\mathbf{r}}_{m,k}, \mathbf{v}_k). \end{aligned} \tag{21}$$

where $\bar{\mathbf{T}}_k$, and $\bar{\mathbf{r}}_{m,k}$ are known signals. In the following, the discrete-time process disturbance $\mathbf{w}_k$ and measurement noise $\mathbf{v}_k$ are assumed to have zero mean.

A. Extended Kalman Filter

Let us denote the covariance matrix of the process disturbance by

$$Q_k = E\{\mathbf{w}_k \mathbf{w}_k'\} \tag{22}$$

and that of the measurement noise by

$$R_k = E\{\mathbf{v}_k \mathbf{v}_k'\}. \tag{23}$$

Since that the error $\mathbf{e}_m$ affects both the dynamic model and the measurement equation, also the cross-covariance between $\mathbf{w}_k$ and $\mathbf{v}_k$, $S_k = E\{\mathbf{w}_k \mathbf{v}_k'\}$, must be considered.

Let $\hat{\mathbf{X}}_k^+$ be the state estimate at time k and let P_k^+ be the estimation error covariance matrix at the same time. Then, the EKF prediction and correction equations are as follows [13].

Prediction

$$\begin{aligned} \hat{\mathbf{X}}_{k+1}^- &= f_d(\hat{\mathbf{X}}_k^+, \bar{\mathbf{T}}_k, \bar{\mathbf{r}}_{m,k}, \mathbf{0}) \\ P_{k+1}^- &= F_k P_k^+ F_k' + G_k Q_k G_k' \end{aligned}$$

Correction

$$\begin{aligned} \hat{\mathbf{X}}_{k+1}^+ &= \hat{\mathbf{X}}_{k+1}^- + K_{k+1}[\mathbf{Y}_{k+1} - h(\hat{\mathbf{X}}_{k+1}^-, \bar{\mathbf{r}}_{m,k+1}, \mathbf{0})] \\ P_{k+1}^+ &= [I - K_{k+1}H_{k+1}]P_{k+1}^- - K_{k+1}V_{k+1}S_k' G_k' \\ K_{k+1} &= [P_{k+1}^- H_{k+1}' + G_k S_k V_{k+1}'][H_{k+1}P_{k+1}^- H_{k+1}' + V_{k+1} R_k V_{k+1}' \\ &\qquad + H_{k+1} G_k S_k V_{k+1}' + V_{k+1} S_k' G_k' H_{k+1}']^{-1} \end{aligned}$$

where the superscript "-" denotes the prediction of the corresponding quantity before the measurement at time $k+1$ is processed, and

$$F_k \triangleq \left.\frac{\partial f_d}{\partial \mathbf{X}}\right|_{\hat{\mathbf{X}}_k^+, \bar{\mathbf{T}}_k, \bar{\mathbf{r}}_{m,k}, \mathbf{0}}, \qquad G_k \triangleq \left.\frac{\partial f_d}{\partial \mathbf{w}}\right|_{\hat{\mathbf{X}}_k^+, \bar{\mathbf{T}}_k, \bar{\mathbf{r}}_{m,k}, \mathbf{0}},$$

$$H_k \triangleq \left.\frac{\partial h}{\partial \mathbf{X}}\right|_{\hat{\mathbf{X}}_k^-, \bar{\mathbf{r}}_{m,k}, \mathbf{0}}, \qquad V_k \triangleq \left.\frac{\partial h}{\partial \mathbf{v}}\right|_{\hat{\mathbf{X}}_k^-, \bar{\mathbf{r}}_{m,k}, \mathbf{0}}.$$

Clearly, if the measurements are available with a frequency lower than the chosen sampling frequency (e.g., every $N\Delta_T$), then the intermediate state estimates are updated according only to the prediction step (i.e., N prediction steps are performed between two consecutive correction steps).

B. Unscented Kalman Filter

The UKF is a recursive state estimator based on the Unscented Transform, which is a method to approximate the mean and covariance of a random variable undergoing a nonlinear transformation [14], [24]. The underlying idea is to estimate the statistics of the transformed variable from a set of $2n+1$ points (called *sigma points*), with n being the dimension of the considered random variable. Sigma points are generated deterministically, on the basis of the (known) covariance matrix of the initial random variable and depending on the parameters of the filter. Unlike the EKF, the UKF does not require the evaluation of the Jacobians of the functions $f_d(\cdot)$ and $h(\cdot)$, since the gains to be used during the estimation are computed directly from the sigma points. Hence, the UKF represents a possible alternative to the EKF whenever a linearized model is not accurate enough or the Jacobian computation becomes too cumbersome (e.g., see [25] for an application of the UKF to the attitude estimation of a multibody satellite).

In the following the UKF update equations are reported for the dynamic model (21) [24]. Let us define the augmented state vector $\mathbf{X}^a = [\mathbf{X}' \ \mathbf{w}' \ \mathbf{v}']' \in \mathbb{R}^L$. Denote by $\hat{\mathbf{X}}_k^a$ and P_k^a the state estimate and the corresponding error covariance matrix

$$\hat{\mathbf{X}}_k^a = [(\hat{\mathbf{X}}_k^+)' \ \mathbf{0} \ \mathbf{0}]' \qquad P_k^a = \begin{bmatrix} P_k^+ & 0 & 0 \\ 0 & Q_k & S_k \\ 0 & S_k' & R_k \end{bmatrix}$$

Sigma-point generation

For $i = 0, \dots, 2L$:

$$\boldsymbol{\chi}^a_{i,k} = \begin{cases} \hat{\mathbf{X}}^a_k & i = 0 \\ \hat{\mathbf{X}}^a_k + \left(\sqrt{(L+\lambda)P^a_k}\right)_i & i = 1, \dots, L \\ \hat{\mathbf{X}}^a_k - \left(\sqrt{(L+\lambda)P^a_k}\right)_{i-L} & i = L+1, \dots, 2L \end{cases}$$

$$\triangleq [(\boldsymbol{\chi}^x_{i,k})' \ (\boldsymbol{\chi}^w_{i,k})' \ (\boldsymbol{\chi}^v_{i,k})']'$$

where $(P)_i$ denotes the i-th column of matrix P.

Prediction

$$\begin{aligned}
\boldsymbol{\chi}^x_{i,k+1|k} &= f_d(\boldsymbol{\chi}^x_{i,k}, \bar{\mathbf{T}}_k, \bar{\mathbf{r}}_{m,k}, \boldsymbol{\chi}^w_{i,k}, k) \qquad i = 0, \dots, 2L \\
\hat{\mathbf{X}}^-_{k+1} &= \sum_{i=0}^{2L} W_i^{(m)} \boldsymbol{\chi}^x_{i,k+1|k} \\
P^-_{k+1} &= \sum_{i=0}^{2L} W_i^{(c)} [\boldsymbol{\chi}^x_{i,k+1|k} - \hat{\mathbf{X}}^-_{k+1}][\boldsymbol{\chi}^x_{i,k+1|k} - \hat{\mathbf{X}}^-_{k+1}]' \\
\boldsymbol{\mathcal{Y}}_{i,k+1|k} &= h(\boldsymbol{\chi}^x_{i,k+1|k}, \bar{\mathbf{r}}_{m,k+1}, \boldsymbol{\chi}^v_{i,k}) \qquad i = 0, \dots, 2L \\
\hat{\mathbf{Y}}^-_{k+1} &= \sum_{i=0}^{2L} W_i^{(m)} \boldsymbol{\mathcal{Y}}_{i,k+1|k}
\end{aligned}$$

Correction

$$\begin{aligned}
P_{YY} &= \sum_{i=0}^{2L} W_i^{(c)} [\boldsymbol{\mathcal{Y}}_{i,k+1|k} - \hat{\mathbf{Y}}^-_{k+1}][\boldsymbol{\mathcal{Y}}_{i,k+1|k} - \hat{\mathbf{Y}}^-_{k+1}]' \\
P_{XY} &= \sum_{i=0}^{2L} W_i^{(c)} [\boldsymbol{\chi}^x_{i,k+1|k} - \hat{\mathbf{X}}^-_{k+1}][\boldsymbol{\mathcal{Y}}_{i,k+1|k} - \hat{\mathbf{Y}}^-_{k+1}]' \\
\hat{\mathbf{X}}^+_{k+1} &= \hat{\mathbf{X}}^-_{k+1} + P_{XY} P_{YY}^{-1} (\mathbf{Y}_{k+1} - \hat{\mathbf{Y}}^-_{k+1}) \\
P^+_{k+1} &= P^-_{k+1} - P_{XY} P_{YY}^{-1} P'_{XY}
\end{aligned}$$

The weights $W_i^{(\cdot)}$ are computed as follows

$$\begin{aligned}
W_0^{(m)} &= \tfrac{\lambda}{L+\lambda}, \quad W_0^{(c)} = \tfrac{\lambda}{L+\lambda}(1 - \alpha^2 + \beta), \\
W_i^{(m)} &= W_i^{(c)} = \tfrac{1}{2(L+\lambda)}, \quad i = 1, \dots, 2L
\end{aligned}$$

where $\lambda = \alpha^2(L+\kappa) - L$, and $\alpha,\ \beta$ and κ are the tuning parameters of the filter.

C. *Filter covariances*

In this section, the covariances of process disturbance $\mathbf{w}_k$ and of the measurement noise $\mathbf{v}_k$ used in the filters are reported. By recalling the definition (10), under the assumption that $\bar{\mathbf{w}}_k$, $\omega_{u,k}$, $\mathbf{e}_{m,k}$ are uncorrelated stochastic processes, the covariance matrix Q_k in (22) is block diagonal

$$Q_k = \text{diag}([Q_{\bar{\mathbf{w}}},\ \sigma_u^2,\ S_{\mathbf{e}_m}])$$

where $Q_{\bar{\mathbf{w}}},\ \sigma_u^2,\ S_{\mathbf{e}_m}$, are the covariances of the stochastic processes $\bar{\mathbf{w}},\ \omega_u,\ \mathbf{e}_m$, respectively.

Recall that the process disturbance $\bar{\mathbf{w}}$ accounts for neglected forces acting on the spacecraft. In order to model such effects, the covariance $Q_{\bar{\mathbf{w}}}$ is taken as the sum of three terms (which basically means to assume that the corresponding error sources are independent)

$$Q_{\bar{\mathbf{w}}} = Q_e + Q_m + Q_t.$$

where Q_e and Q_m are due to the Earth and Moon gravitational field asymmetry, while Q_t takes into account other unmodeled effects, like air drag and sun attraction.

Matrix Q_e has been estimated by evaluating the difference between the gravitational force predicted by the nominal model $\frac{\mu}{\rho^3}\mathbf{r}$ and the one yielded by the Earth gravitational model JGM-2 [26]. For each fixed value of ρ, the sample standard deviation has been computed at 900 different spacecraft positions, uniformly distributed on a sphere of radius ρ centered at the Earth. This results in an estimated covariance matrix depending on the distance of the spacecraft to the earth

$$Q_e = \text{diag}\left(\left[\frac{2.82 \cdot 10^{20}}{\rho^8},\ \frac{2.82 \cdot 10^{20}}{\rho^8},\ \frac{7.34 \cdot 10^{20}}{\rho^8}\right]\right) \quad \frac{km^2}{s^4}.$$

The same has been done for the Moon gravitational field asymmetry, by considering the model LP-150 [27]. The standard deviations of the modeled disturbance as a function of ρ_{sm} has been estimated, giving a covariance matrix

$$Q_m = \frac{10^{18}}{\rho_{sm}^8} I_{3\times 3} \quad \frac{km^2}{s^4},$$

where $I_{3\times 3}$ is the identity matrix of order 3. The value of the covariance Q_t has been chosen as $Q_t = \sigma_t^2 I_{3\times 3}$, where σ_t^2 plays the role of a tuning knob in the design of the filters. The variance of the input perturbation ω_u is set to $\sigma_u^2 = 0.01^2$. Finally, the error covariance of the Moon ephemerides algorithm has been chosen as $S_{\mathbf{e}_m} = 10^2 I_{3\times 3}\ km^2$ [28].

Assuming that the measurement errors $\mathbf{n}_k$ in (18) are uncorrelated and independent of $\mathbf{e}_{m,k}$, $\mathbf{v}_k$ in (19) can be modeled as a white stochastic process with block diagonal covariance matrix (23) given by

$$R_k = \text{diag}([\sigma_v^2 I_{4\times 4},\ S_{\mathbf{e}_m}]),$$

where σ_v^2 depends on the sensor accuracy.

Finally, the cross-covariance between $\mathbf{w}_k$ and $\mathbf{v}_k$ is given by

$$S_k = \begin{bmatrix} 0_{10\times 4} & 0_{10\times 3} \\ 0_{3\times 4} & S_{\mathbf{e}_m} \end{bmatrix}.$$

IV. Simulation results

In this section, the performance of the filters is evaluated by simulating two transfer missions, namely a Earth-to-Moon transfer and a geostationary orbit raising.

The sampling time used to discretize the dynamic model (4) is $\Delta_T = 15\ s$ and the angular measurements (20) are supposed to be available once per hour. This means that both filters perform a correction step every 240 prediction steps. The standard deviation σ_t of the disturbance ω_t acts as a tuning parameter of both filters. The standard deviation of the angular measurement errors is supposed to be $\sigma_v = 0.01\frac{\pi}{180}\ rad$, according to the accuracy of several off-the-shelf sensors employed in celestial navigation (see e.g. [3], [11], [12]).

For each filter both the estimation errors and the corresponding standard deviations are evaluated by comparing the state estimates to the output of an accurate mission simulator, which explicitly accounts for a number of perturbing effects. In the simulator, the gravitational field asymmetry of Earth and Moon is considered through the JGM-2 and LP-150 models, respectively. A point-mass approximation is adopted to model the Sun attraction on the spacecraft. The "cannonball model" is used to take into account the effect of the solar radiation pressure. The J71 atmospheric model accounts for air drag. Finally, the resulting differential equations modeling the spacecraft dynamics, and including all the above orbital perturbations, are integrated through a fifth-order Runge-Kutta method.

A. Earth-to-Moon transfer mission

In the example of Earth-to-Moon transfer mission considered, the initial orbit has the following parameters: eccentricity $e = 0.5$, inclination $i = 10^o$, altitude perigee $a = 3 \cdot 10^4\ km$. The forcing input is a continuous thrust tangential to the trajectory, with

$$\mathbf{T} = T\frac{\dot{\mathbf{r}}}{\|\dot{\mathbf{r}}\|}, \tag{24}$$

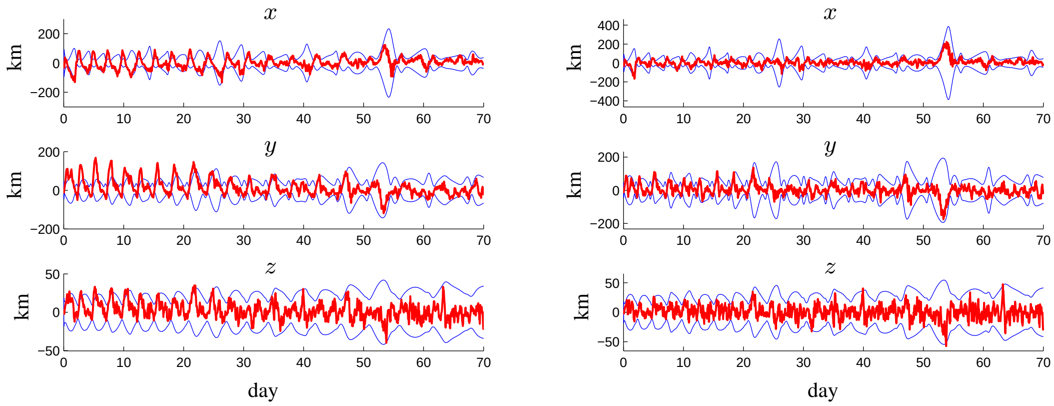

(a) EKF (b) UKF

Fig. 3. Earth-to-Moon transfer mission: x, y, z estimation errors (thick line) and 99% confidence intervals (thin line).

and $T = 0.05\ N$. Results are reported for 70 days of mission, with the spacecraft reaching a final apogee altitude of $2.04 \cdot 10^5\ km$.

Both filters have been initialized with the same initial estimate and covariance matrix:

$$\hat{\mathbf{X}}_0^+ = \mathbf{X}(0)$$
$$P_0^+ = \text{diag}\left(\left[1\ km^2,\ 1\ km^2,\ 1\ km^2,\ 10^{-4}\ \frac{km^2}{s^2},\ 10^{-4}\ \frac{km^2}{s^2}, 10^{-4}\ \frac{km^2}{s^2},\ 10^{-6}\ kg^2\right]\right),$$

where $\mathbf{X}(0)$ denotes the true initial state vector (see equation (3)).

For the EKF, the standard deviation of the process disturbance ω_t has been tuned to $\sigma_t = 10^{-5}\ \frac{km}{s^2}$. Smaller values of σ_t resulted in a significant lack of consistency of the filter (estimation errors remarkably outside the 99% confidence intervals). Figure 3(a) shows the EKF estimation errors for coordinates x, y, z, and the corresponding 99% confidence intervals. In the first column of Table I the sample standard deviation of the estimation errors are reported (results are averaged over 10 simulation runs). The overall average localization error turns out to be $48.82\ km$.

For the UKF, the following parameters have been used for the generation of the *sigma* points: $\alpha = 10^{-3}$, $\kappa = 0$, $\beta = 2$. The standard deviation of the process disturbance ω_t has been tuned to $\sigma_t = 10^{-7}\ \frac{km}{s^2}$. In Figure 3(b) the x, y, z estimation errors and the 99%, confidence intervals are shown. The second column of Table I reports the sample standard deviation of the estimation errors, averaged over 10 simulation runs. The overall average localization error is now $38.00\ km$, with a reduction of about 20% with respect to the EKF. Moreover, Figures 3(a)-3(b) show that UKF features better consistency properties (error almost always inside the 99% confidence intervals). Notice that these results have been obtained with a value of σ_t smaller than that used by the EKF.

	EKF	UKF
x (km)	36.80	31.59
y (km)	42.55	31.57
z (km)	10.81	10.94
$\dot{x}$ (km/s)	$1.33 \cdot 10^{-3}$	$1.07 \cdot 10^{-3}$
$\dot{y}$ (km/s)	$1.51 \cdot 10^{-3}$	$1.18 \cdot 10^{-3}$
$\dot{z}$ (km/s)	$3.43 \cdot 10^{-4}$	$4.48 \cdot 10^{-4}$

TABLE I

EARTH-TO-MOON TRANSFER MISSION: SAMPLE STANDARD DEVIATION OF ESTIMATION ERRORS.

Also the relative position of Earth, Moon and spacecraft influences the magnitude of the localization error. Intuition suggests that larger errors can be expected in those configurations in which the three bodies are aligned, due to poor geometry for angle measurement. This is confirmed by Figure 4, where the estimated root mean square localization error (RMSE) is plotted against the alignment angle (i.e., the angle between the spacecraft and Moon directions, as seen from the Earth). The figure refers to the UKF , but a similar phenomenon occurs for EKF. The error peaks are mostly grouped around angles zero (Moon and Earth aligned on opposite side respect to the spacecraft) and $\pm\pi$ (Moon and Earth aligned on the same side respect to the spacecraft). Conversely, the smallest values correspond to angles close to $\pm\frac{\pi}{2}$.

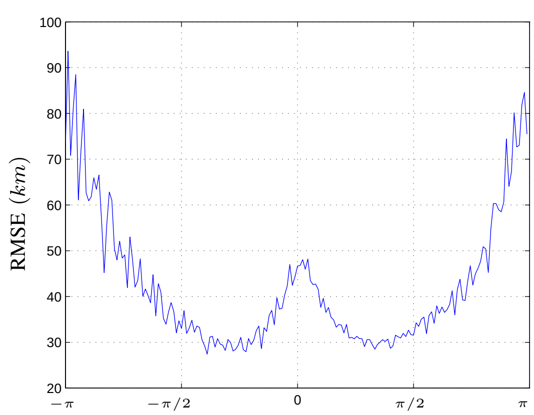

Fig. 4. Root mean square error of position estimation vs. spacecraft-Earth-Moon alignment

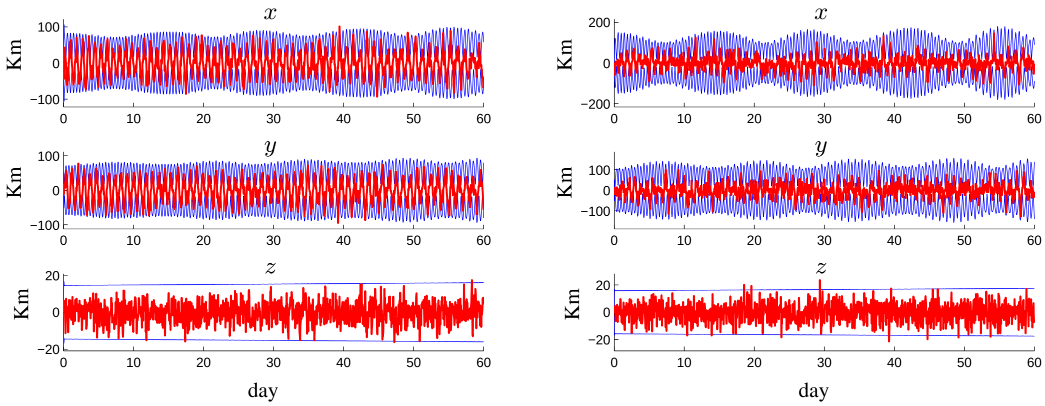

(a) EKF (b) UKF

Fig. 5. GEO orbit raising: x, y, z estimation errors (thick line) and 99% confidence intervals (thin line).

B. GEO Transfer

The second mission considered is the final stint of a chemical-electric orbit raising (C-EOR) to geostationary orbit [6], [29] (GEO). The initial orbit is characterized by low eccentricity and inclination, altitude perigee $a = 3 \cdot 10^4\ km$ and initial spacecraft mass of $1.5 \cdot 10^3\ kg$. The control strategy is again a continuous thrust tangential to the trajectory as in (24), with $T = 0.05\ N$. The autonomous navigation algorithm was tested for a period of 60 days of mission, sufficient to complete the satellite orbit raising to GEO.

The parameters of the filters have been chosen as in the Earth-to-Moon transfer mission, except for σ_t. For the EKF algorithm the standard deviation associated with the parameter ω_t has been tuned to $\sigma_t = 10^{-4}\ \frac{km}{s^2}$, whereas in the UKF algorithm the value $\sigma_t = 10^{-6}\ \frac{km}{s^2}$ was used. Values of σ_t smaller than 10^{-4} led to inconsistent EKF estimates, with estimation errors significantly outside the 99% confidence intervals.

In Figure 5(a) EKF simulation results are shown. The estimation errors and the corresponding 99% confidence intervals for satellite position are plotted. The sample standard deviation of the estimation errors, averaged over 10 simulation runs, is reported in the first column of Table II. The overall average position errors resulted to be $40.8\ km$.

Figure 5(b) and the second column of Table II show the position estimation errors and the sample standard deviation (averaged over 10 runs) for the UKF algorithm. In this case the overall average position errors are $36.2\ km$. As far as the localization error is concerned, the UKF provides a 10% improvement. It is worth remarking that running the EKF with the tuning parameter $\sigma_t = 10^{-6}\ \frac{km}{s^2}$ (i.e., the same value

	EKF	UKF
x (km)	32.02	31.02
y (km)	31.27	30.17
z (km)	5.47	6.16
$\dot{x}$ (km/s)	$3.2 \cdot 10^{-3}$	$3.7 \cdot 10^{-3}$
$\dot{y}$ (km/s)	$3.2 \cdot 10^{-3}$	$3.7 \cdot 10^{-3}$
$\dot{z}$ (km/s)	$0.9 \cdot 10^{-3}$	$1.7 \cdot 10^{-3}$

TABLE II

GEO ORBIT RAISING: SAMPLE STANDARD DEVIATION OF ESTIMATION ERRORS

used for the UKF) results in a complete lack of filter consistency, and the average estimation error turns out to increase of one order of magnitude.

From Figure 5 it can be observed that the standard deviation of the x and y estimation errors has two characteristic frequencies, the faster one being approximately 2 cycles per day. It is worth noticing that also when the standard deviation is small the estimation error is still within the 3σ bounds, as can be seen in Figure 6(a), where a magnified view of the localization error during the last 10 days of the GEO orbit raising mission is shown.

Also in this kind of mission the spacecraft-Earth-Moon alignment greatly influences the estimation error (see Figure 6(b)). The plot refers to UKF estimate, but a similar behavior is observed also for EKF. The expected error grows as the satellite, the Earth and the Moon approach a collinear configuration, whereas the most accurate estimates are expected when the satellite sees Earth and Moon along orthogonal directions.

V. CONCLUSIONS AND FUTURE WORK

The performance of different nonlinear estimation techniques for the autonomous navigation of spacecraft in low-cost deep space missions has been analyzed. The spacecraft localization problem has been addressed via both the Extended Kalman Filter and the Unscented Kalman Filter. The localization procedure is based only on angular measurements of celestial bodies with respect to the spacecraft reference system, and does not require range measurements which can be difficult to obtain. The behavior of the filters has been tested on two sample missions, using an accurate mission simulator accounting for several perturbing effects. The accuracy of both estimators turned out to be satisfactory, featuring average localization errors which are

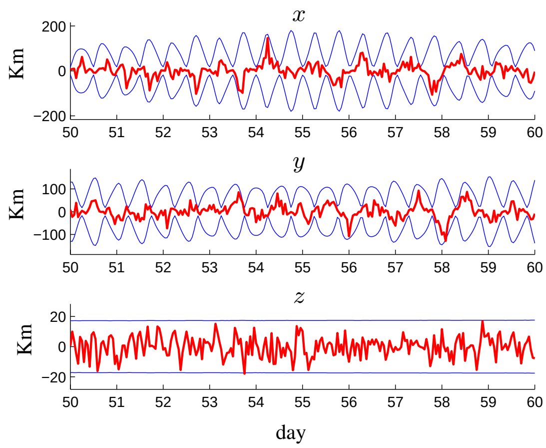

(a)

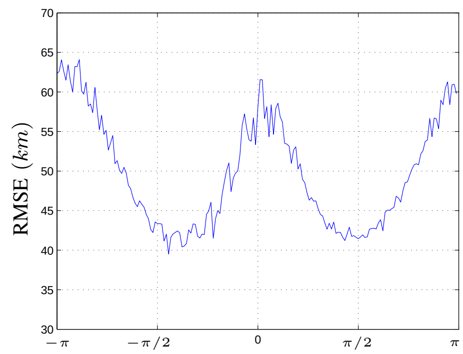

(b)

Fig. 6. (a) Magnified view of UKF localization error during GEO orbit raising. (b) Effect of spacecraft-Earth-Moon alignment on localization error.

reasonably small for the type of missions of interest. Although the filters considered in the paper resulted in localization errors of the same order of magnitude, the UKF has shown better performance in terms of average localization accuracy and consistency of the estimates.

There are currently two main research lines aiming at analyzing more in depth the suitability of the considered filters for autonomous navigation. The first one is the enrichment of the dynamic model, in order to include also the spacecraft attitude among the quantities to be estimated. The second one concerns the adoption of more accurate sensor models, taking into account the error in estimating the center of celestial bodies from images, as well as the adoption of a star-tracker camera for attitude estimation.

REFERENCES

[1] J. Kim and S. Sukkarieh, "Autonomous airborne navigation in unknown terrain environments," *IEEE Transactions on Aerospace and Electronic Systems*, vol. 40, no. 3, pp. 1031–1045, 2004.

[2] T. Upadhyay, S. Cotterill, and A. W. Deaton, "Autonomous GPS/INS navigation experiment for space transfer vehicle," *IEEE Transactions on Aerospace and Electronic Systems*, vol. 29, no. 3, pp. 772–785, 1993.

[3] D. Tuckness and S. Young, "Autonomous navigation for lunar transfer," *Journal of Spacecraft and Rockets*, vol. 32, no. 2, pp. 279–285, March-April 1995.

[4] European Space Agency, "http://www.esa.int/specials/smart-1," 2003.

[5] D. Milligan, D. Gestal, P. Pardo-Voss, O. Camino, D. Estublier, and C. Koppel, "SMART-1 electric propulsion operational experience." in *Proceedings of the 29th International Electric Propulsion Conference*, Princeton, NJ, November 2005.

[6] D. Oh, S. Kimbrel, and M. Martinez-Sanchez, "End-to-End Optimization of Mixed Chemical-Electric Orbit Raising Missions," in *38th AIAA/ASME/SAE/ASEE Joint Propulsion Conference*, Indianapolis, Indiana, July 2002.

[7] A. C. Long, D. Leung, D. Folta, and C. Gramling, "Autonomous navigation of high-Earth satellites using celestial objects and doppler measurements," in *AIAA/AAS Astrodynamics Specialist Conference*, Denver, CO, August 2000.

[8] A. Vallado, *Fundamentals of Astrodynamics and Applications*, 2nd ed. Microcosm Press jointly with Kluwer Academic Publisher, 2001.

[9] J. Salvail and W. Stuiver, "Solar sailcraft motion in Sun-Earth-Moon space with application to lunar transfer from geosynchronous orbit," *Acta Astronautica*, vol. 35, no. 2-3, pp. 215–229, 1995.

[10] J. L. Crassidis, F. L. Markley, and Y. Cheng, "Survey of nonlinear attitude estimation methods," *Journal of Guidance Control and Dynamics*, vol. 30, no. 1, pp. 12–28, 2007.

[11] F. Tai and P. Noerdlinger, "A low cost autonomous navigation system," in *Guidance and control 1989: Proceedings of the Annual Rocky Mountain Guidance and Control Conference*, 1989, pp. 3–23.

[12] R. Hosken and J. Wertz, "Microcosm autonomous navigation system on-orbit operation," *Advances in the Astronautical Sciences*, vol. 88, pp. 491–491, 1995.

[13] J. Crassidis and J. Junkins, *Optimal Estimation of Dynamic Systems*, ser. Applied mathematics and nonlinear science series. Chapman & Hall/CRC, 2004.

[14] S. J. Julier and J. K. Uhlmann, "A new extension of the Kalman filter to nonlinear systems," in *Proceedings of AeroSense: The 11th Int. Symp. on Aerospace/Defence Sensing, Simulation and Controls*, 1997, pp. 182–193.

[15] A. Farina, B. Ristic, and D. Benvenuti, "Tracking a ballistic target: comparison of several nonlinear filters," *IEEE Transactions on Aerospace and Electronic Systems*, vol. 38, no. 3, pp. 854–867, 2002.

[16] R. Zhan and J. Wan, "Iterated Unscented Kalman Filter for Passive Target Tracking," *IEEE Transactions on Aerospace and Electronic Systems*, vol. 43, no. 3, pp. 1155–1163, 2007.

[17] M. St-Pierre and D. Gingras, "Comparison between the unscented Kalman filter and the extended Kalman filter for the position estimation module of an integrated navigation information system," in *2004 IEEE Intelligent Vehicles Symposium*, 2004, pp. 831–835.

[18] Y. Yudan and D. A. Grajner-Brzezinska, "Nonlinear Bayesian filter: Alternative ti the Extended Kalma Filter in the GPS/INS fusion systems," in *Proceedings of the ION GNSS 18th Internetional Technical Meeting of the Satellite Division*, 13-16 September 2005, pp. 1391–1400.

[19] J. LaViola Jr, "A comparison of unscented and extended Kalman filtering for estimating quaternion motion," in *Proceedings of the 2003 American Control Conference*, vol. 3, 2003, pp. 2435– 2440.

[20] N. Ceccarelli, A. Garulli, A. Giannitrapani, M. Leomanni, and F. Scortecci, "Spacecraft localization via angle measurements for autonomous navigation in deep space." in *Proceedings of the 17th IFAC Symposium on Automatic Control in Aerospace.*, Toulouse, FR, June 2007.

[21] J. R. F. M. D. Griffin, *Space Vehicle Design*, 2nd ed., ser. AIAA education. AIAA, 2004.

[22] S. Sarkka, "On Unscented Kalman Filtering for state estimation of continuous-time nonlinear systems," *IEEE Transactions on Automatic Control*, vol. 52, no. 9, pp. 1631–1641, 2007.

[23] D. King-Hele, *Satellite Orbits in an Atmosphere: Theory and Applications*. Springer, 1987.

[24] E. Wan and R. van der Merwe, "The Unscented Kalman Filter," in *Kalman Filtering and Neural Networks*, S. Haykin, Ed. Wiley, 2001, ch. 7, pp. 221–280.

[25] J. Fisher and S. R. Vadali, "Gyroless attitude control of multibody satellites using an unscented kalman filter," *Journal of Guidance Control and Dynamics*, vol. 31, pp. 245–251, 2008.

[26] European Cooperation for Space Standardization, "Space engineering," 2200 AG Noordwijk, THe Netherlands, 2000.

[27] A. Konopliv, S. Asmar, E. Carranza, W. Sjogren, and D. Yuan, "Recent gravity models as a result of the lunar prospector mission," *Icarus*, vol. 150, pp. 1–18, Mar. 2001.

[28] P. Seidelmann, E. Santoro, and K. Pulkkinen, "Systematic differences between planetary observations and ephemerides," in *Second U. S. Hungary Workshop*, ser. Dynamical Astronomy. Univ. of Texas Press, September 1985, pp. 55–65.

[29] R. Killinger, R. Kukies, M. Surauer, H. Gray, and G. Saccoccia, "Final Report on the ARTEMIS Salvage Mission Using Electric Propulsion," in *39th AIAA/ASME/SAE/ASEE Joint Propulsion Conference and Exhibit*, Huntsville, Alabama, July 20-23 2003.

Antonio Giannitrapani was born in Salerno, Italy, in 1975. He received the Laurea degree in Computer Engineering in 2000, and the Ph.D. in Control Systems Engineering in 2004, both from the Università di Siena. In 2005 he joined the Dipartimento di Ingegneria dell'Informazione of the same University, where he is currently Assistant Professor of Robotics. His research interests include localization and map building for mobile robots, collective motion for teams of autonomous agents, nonlinear estimation techniques for autonomous navigation, mobile haptic interfaces.

Nicola Ceccarelli was born in Pisa, Italy, in 1977. He received both Master ('02) degree and Ph.D. ('06) degree from the Università di Siena at the Dipartimento di Ingegneria dell'Informazione. His research activity has dealt with mobile robotics, satellite systems and unmanned aerial vehicles. Form 2006 to 2007 he has been Visiting Scientist at the Air Force Research Laboratory thanks to an award from the U.S. National Research Council. He is currently with GE Oil&Gas as Lead Engineer/Technologist. His duties are mainly focused on simulation and modeling of compressor train systems.

Fabrizio Scortecci received a MS in Aerospace Engineering at the Università di Pisa in 1990. Since his graduation he worked as Researcher and then as a Project Manager in various theoretical and experimental projects related to electric satellite propulsion, aerothermodynamics and spacecraft systems. During the year 2000 he joined AEROSPAZIO Tecnologie s.r.l. working as Senior Scientist and Manager on programs related to on-orbit application of electric propulsion.

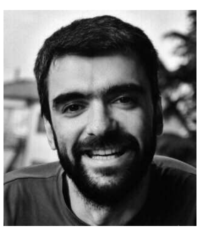

Andrea Garulli was born in Bologna, Italy, in 1968. He received the Laurea in Electronic Engineering from the Università di Firenze in 1993, and the Ph.D. in System Engineering from the Università di Bologna in 1997. In 1996 he joined the Dipartimento di Ingegneria dell'Informazione of the Universit di Siena, where he is currently Professor of Control Systems. He has been member of the Conference Editorial Board of the IEEE Control Systems Society and Associate Editor of the IEEE Transactions on Automatic Control. He currently serves as Associate Editor for the Journal of Control Science and Engineering. He is author of more than 120 technical publications; co-editor of the books "Robustness in Identification and Control", Springer 1999, and "Positive Polynomials in Control", Springer 2005; co-author of the book "Homogeneous Polynomial Forms for Robustness Analysis of Uncertain Systems", Springer 2009. His present research interests include system identification, robust estimation and filtering, robust control, mobile robotics and autonomous navigation.